

# Self-Learning-Based Optimization for Free-form Pipe Routing in Aeroengine with Dynamic Design Environment

Caicheng Wang<sup>1</sup>, Zili Wang<sup>1,2\*</sup>, Shuyou Zhang<sup>1,2</sup>, Yongzhe Xiang<sup>1</sup>, Zheyi Li<sup>1</sup>, Jianrong Tan<sup>1,2</sup>

(1. State Key Laboratory of Fluid Power and Mechatronic Systems, Zhejiang University, Hangzhou, 310027, China. 2. Engineering Research Center for Design Engineering and Digital Twin of Zhejiang Province, Zhejiang University, Hangzhou, 310027, China)

E-mail address: [12425135@zju.edu.cn](mailto:12425135@zju.edu.cn) (Caicheng Wang), [ziliwang@zju.edu.cn](mailto:ziliwang@zju.edu.cn) (Zili Wang), [zsy@zju.edu.cn](mailto:zsy@zju.edu.cn) (Shuyou Zhang), [xyz2022@zju.edu.cn](mailto:xyz2022@zju.edu.cn) (Yongzhe Xiang), [12325137@zju.edu.cn](mailto:12325137@zju.edu.cn) (Zheyi Li), [egi@zju.edu.cn](mailto:egi@zju.edu.cn) (Jianrong Tan)

\*Corresponding author: [ziliwang@zju.edu.cn](mailto:ziliwang@zju.edu.cn) (Zili Wang)

## Abstract:

Pipe routing is a highly complex, time-consuming, and no-deterministic polynomial-time hard (NP-hard) problem in aeroengine design. Despite extensive research efforts in optimizing constant-curvature pipe routing, the growing demand for free-form pipes poses new challenges. Dynamic design environments and fuzzy layout rules further impact the optimization performance and efficiency. To tackle these challenges, this study proposes a self-learning-based method (SLPR) for optimizing free-form pipe routing in aeroengines. The SLPR is based on the proximal policy optimization (PPO) algorithm and integrates a unified rule modeling framework for efficient obstacle detection and fuzzy rule modeling in continuous space. Additionally, a potential energy table is constructed to enable rapid queries of layout tendencies and interference. The agent within SLPR iteratively refines pipe routing and accumulates the design knowledge through interaction with the environment. Once the design environment shifts, the agent can swiftly adapt by fine-tuning network parameters. Comparative tests reveal that SLPR ensures smooth pipe routing through cubic non-uniform B-spline (NURBS) curves, avoiding redundant pipe segments found in constant-curvature pipe routing. Results in both static and dynamic design environments demonstrate that SLPR outperforms three representative baselines in terms of the pipe length reduction, the adherence to layout rules, the path complexity, and the computational efficiency. Furthermore, tests in dynamic environments indicate that SLPR eliminates labor-intensive searches from scratch and even yields superior solutions compared to the retrained model. These results highlight the practical value of SLPR for real-world pipe routing, meeting lightweight, precision, and sustainability requirements of the modern aeroengine design.

*Keywords:* Layout optimization; Pipe routing; Aerospace components; Deep Reinforcement learning; Proximal policy optimization.

## 1. Introduction

Recent advancements in the aerospace industry have raised higher demand for efficient pipe routing to achieve lightweight, precision, and sustainability in aeroengine design. As the foundation for all other detailed designs, pipe routing holds high research significance and practical value. Typically, pipe routing in an aeroengine requires the precise arrangement of hundreds of pipes while avoiding interference [1]. This complexity renders it a nondeterministic polynomial-time hard (NP-hard) problem. Currently, the pipe routing is primarily accomplished manually with the assistance of computer-aided design (CAD) software, a process that can be time-consuming, inefficient, and labor-intensive [2]. The working hours spent on pipe routing generally occupy more than 50% of the total detail-design man-hours [3]. These high costs have spurred a surge of research into automated pipe routing (APR) [4].

The APR problem can be classified as a type of path planning problem [5], focusing on determining the shortest, collision-free paths for pipes connecting endpoints within narrow three-dimensional spaces. Traditional APR approaches often utilize constant-curvature pipes, with pipe paths represented as simple polylines. However, as aeroengine designs become increasingly complex, the available space within the engine is significantly constrained, making constant-curvature pipe routing inefficient because of excessive material use and space occupancy. This shift has driven the adoption of free-form pipes [6], whose axes are represented by spline curves, allowing more flexible obstacle avoidance and reduced pipe length [7]. Nevertheless, this high degree of design flexibility also introduces new challenges for APR research.

The procedures of APR involve environment modeling, rules modeling, and route searching [8, 9]. Environment modeling refers to the organization and utilization of the layout space [10]. Most existing methods simplify this process through discrete space modeling, which divides the continuous routing space and obstacles into discrete units. Although discrete space modeling is easy to implement and convenient for path searching, its accuracy and flexibility are constrained by grid size, limiting the adaptability of free-form pipe routing. In this context, continuous space modeling is more appropriate for free-form pipe routing, as it allows exploration at any point in space. Within continuous space, collision detection is generally challenging due to the irregular shape of obstacles [11]. Beyond obstacle avoidance, pipe routing must adhere to various constraints related to functionality, installation, aesthetics, reliability, and maintenance of the piping system [9]. Such layout rules are often fuzzy, making them difficult to represent mathematically in continuous space. Additionally, aeroengine pipe routing can involve dozens or even hundreds of rules, with customization requirements adding unique rules for different engines, making it impractical to model each rule individually. Given these challenges, an efficient, accurate, and unified framework for rule modeling in continuous space is essential.

Various route search methods have been developed over the years to find optimal layouts in complex environments with multiple constraints. Traditional search algorithms use point-to-point traversal or sampling to find the optimal path between the start and the target [12]. Although efficient for certain 2D searches, these algorithms often struggle in large or complex 3D environments. Heuristic-based optimization techniques, inspired by genetic principles or the collective behaviors of organisms, offer advantages such as high parallelism, self-organization, and ease of implementation, making them the most frequently used methods in route search [13]. However, these methods tend to be computationally intensive, prone to getting stuck in local optima [14], and sensitive to the selection of initial parameters [15]. Additionally, both traditional and heuristic-based algorithms lack learning capabilities, requiring a fresh search from scratch for each new task or environment. In contrast, reinforcement learning (RL) algorithms offer a more adaptive, learning-based approach [16]. RL methods allow agents to learn through interactions with the environment and generalize learned behaviors to unseen scenarios [17, 18]. Although rarely applied to pipe routing, RL approaches are well-suited for aeroengine piping, where frequent design modifications often require extensive adjustments to existing routes.

Given these gaps, this study proposes a self-learning approach for free-form pipe routing in aeroengines. First, a unified rule modeling framework and a potential energy table are introduced. The learning-based path planning algorithm, proximal policy optimization (PPO) [19], is then integrated with non-uniform B-spline (NURBS) curves to implement free-form pipe routing and adapt to frequent environmental changes. To sum up, the key contributions of this study are as follows:

- 1) Existing constant-curvature pipe routing methods result in excessive space occupancy and material waste. In this regard, an APR method for free-form pipe routing using NURBS curves is developed to meet the lightweight, precision, and sustainability demands of modern aeroengine design.

2) A unified rule modeling framework in continuous space is proposed to efficiently and accurately represent collisions and layout preferences while allowing the flexible integration of new rules. Based on this framework, a potential energy table is constructed to enable efficient and precise querying of interference and layout tendencies through a spatial mapping relationship.

3) The learning-based algorithm, PPO, is integrated into the layout process. Through interactions with the environment and fine-tuning, the agent learns to achieve flexible obstacle avoidance and adapt to changes in the environment.

The remainder of this study is organized as follows: Section 2 reviews the related work. Section 3 defines the problem of pipe routing as a RL task. Section 4 details the self-learning pipe routing framework proposed in this study. Section 5 evaluates the effectiveness of the framework through comparative experiments. Finally, Section 6 presents the conclusion.

## 2. Related work

### 2.1. Modeling of environment and rules

Environment modeling methods in pipe routing are generally classified into continuous space modeling and discrete space modeling, with the latter being the most commonly used. In discrete space modeling, both the layout space and obstacles are divided into a number of discrete units. For instance, the raster method divides the layout space into uniform cubic grids, where grids containing obstacles are assigned a value of one, while free grids are assigned a value of zero [20]. The pipe path is then represented by a start point, an end point, and a sequence of grids connecting them. This method is particularly convenient for orthogonal pipe routing and thus is widely used in shipbuilding [21] and factory layouts [22], where orthogonal pipes are preferred. In aeroengine pipe routing, where the space between the engine casing and the nacelle forms a rotational annular space, fan grids are commonly used to divide the layout space [23]. However, for free-form pipes, whose axes are typically represented by spline curves, layout space requires higher degrees of freedom and accuracy. Although paths generated in discrete space can be fitted with B-spline curves to create free and smooth paths [24], this fitting introduces deviations from the original path, necessitating secondary collision detection and evaluation. Research has also explored using the rapidly-exploring random tree star (RRT\*) algorithm to directly identify control points for quadratic B-spline curves in smooth path planning [25], but its application has been limited to two dimensions, with reduced flexibility for three-dimensional pipe routing.

Collision avoidance is the fundamental rule in pipe routing. Methods such as bounding boxes and voxel-based representations are commonly employed to simplify collision detection [26]. Bounding boxes, such as axis-aligned bounding box, sphere, and oriented bounding box, provide approximate collision detection by enclosing objects within simple geometric shapes [27]. For more complex objects, the octree structure is the widely used, which divide space into eight equivalent subspaces to enhance detection efficiency [28]. In addition to obstacle avoidance, the pipe routing contains many fuzzy rules, which are elastic or ambiguous and difficult to define by explicit mathematical expressions. For instance, pipe routing rules may require pipes to be positioned as close as possible to obstacles and routing boundaries [29]. In discrete space modeling, potential energy methods are commonly used to express fuzzy preferences, by assigning low potential values to cells that favor pipe layouts and high values to unfavorable ones [30]. However, such fuzzy preferences are difficult to represent mathematically in continuous space. Furthermore, there exists multiplicity and customizability of pipe routing rules, making it impractical to model each rule individually.

Free pipe in aeroengines offers promising advantages but presents challenges in environment and rule modeling within continuous space. Drawing on existing research, this study introduces a unified, flexible rule modeling framework for free pipe routing using the NURBS curve in continuous 3D space. Moreover, a potential energy table is constructed to efficiently query interference and pipe routing preferences.

### 2.2. Route search methods

Recent years have witnessed significant advancements in route search methods [31]. Broadly, route search methods can be classified into traditional search algorithms, heuristic-based optimization algorithms, and learning-based algorithms. Traditional search algorithms employ point-to-point traversal, such as the Dijkstra algorithm [32] and A\* algorithm [33], or sampling methods like RRT [34], to identify optimal routes. Heuristic-based optimization techniques include evolutionary algorithms, such as genetic algorithms [35], and swarm intelligence algorithms, such as particle swarm optimization [36], and ant colony optimization [37].

Although widely applied, these methods are inefficient in large, complex 3D spaces and must restart the search from scratch for each new routing task and new environment. The learning-based algorithm, particularly RL methods, addresses these limitations by learning and adapting through interactions with the environment. For continuous tasks, policy-based algorithms such as soft actor-critic (SAC) [38] and PPO [19] are commonly used, allowing direct mapping from an environmental state to a continuous action space. RL has been successfully applied in diverse path-planning tasks, such as for autonomous underwater vehicles and UAVs in simple, complex, or dynamically changing environments [39-41]. However, the application of RL in pipe routing remains rare. While PPO combined with curriculum learning has been applied to pipe routing in ships, its application has been confined to orthogonal pipes and discrete space [42]. The potential of PPO still deserves further exploration, especially for free pipe routing of aeroengines in continuous space.

### 3. Problem formulation

#### 3.1. Aeroengine pipe routing

Aeroengine pipe routing refers to identifying a collision-free path between the casing and the nacelle, connecting the designated start and target points. Pipes in aeroengines are typically classified into two types: constant-curvature bent pipes and free-form pipes. The constant-curvature bent pipes, commonly formed by the rotary draw bending process, are the most commonly used. As modern aeroengines move towards lightweight, precision, and sustainability, the demand for free-form pipes has increased dramatically. As illustrated in Fig. 1, both types of pipe paths can be represented as a sequence of axial points as follows:

$$P = \{P_s, P_0, P_1, \dots, P_n, P_t\} \quad (1)$$

where  $P_s$  denotes the start point,  $P_t$  is the target point, and  $P_i = (x_i, y_i, z_i)_{0 \leq i \leq n}$  denotes the connection points to be determined. The axial points represent either bend points for a constant-curvature pipe or control points for a free-form pipe, depending on the pipe type. The curve generated from these axial points forms a collision-free path that adheres to routing constraints. The pipe geometry is then constructed by sweeping a circular profile of diameter  $d$  along this curve.

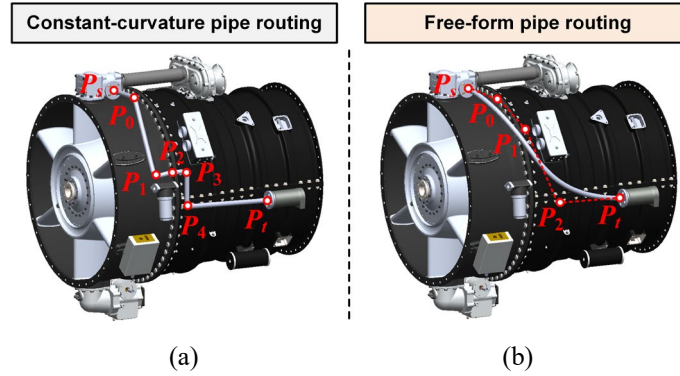


**Fig. 1.** Constant-curvature pipe routing and free-form pipe routing in aeroengine. (a) Constant-curvature pipe routing; (b) Free-form pipe.

Given a series of axial points, a parametric curve can be utilized to generate a continuous path for the free-form pipe. As one of the most popular industry standards, NURBS curves are widely used in path descriptions because of their precise analytical representation and local tuning capabilities [43]. The NURBS curve can be mathematically expressed as:

$$C(u) = \frac{\sum_{i=0}^n N_{i,p}(u)w_i P_i}{\sum_{i=0}^n N_{i,p}(u)w_i}, u \in [0,1] \quad (2)$$

where  $u$  is the curve parameter,  $w_i$  is the weight of the  $i$ -th control point  $P_i$ , and  $N_{i,p}(u)$  is the corresponding basis function, computed based on the knot vector  $U$  and the curve degree  $p$ . Assume that  $U$  is a set of  $m+1$  non-decreasing numbers  $\{u_0, u_1, \dots, u_m\}$ , the  $i$ -th basis function  $N_{i,p}(u)$  is defined recursively as follows:

$$N_{i,0}(u) = \begin{cases} 1 & \text{if } u_i \leq u \leq u_{i+1} \\ 0 & \text{otherwise} \end{cases} \quad (3)$$

$$N_{i,p}(u) = \frac{u - u_i}{u_{i+p} - u_i} N_{i,p-1}(u) + \frac{u_{i+p+1} - u}{u_{i+p+1} - u_{i+1}} N_{i+1,p-1}(u) \quad (4)$$

### 3.2. Reinforcement learning task

The objective of pipe routing is to determine an optimal set of axial control points, and thus it can be formulated as a RL task. In RL, the learner and decision maker are called the agent, while everything it interacts with, comprising all external factors, is referred to as the environment [44]. The RL task is essentially a sequential decision-making problem, commonly represented as a Markov decision process, defined by  $M = (S, A, T_s, R, \gamma)$ . Here, state  $s \in S$  indicates the position and information of the current axial control point within the environment during the routing process. The action  $a \in A$  represents the decision to move from the current control point  $P_i$  to the next control point. When the agent takes action  $a$  in the current state  $s$ , it transitions to the next state  $s'$  according to the state transition function  $T_s(s'|s, a)$  and receives a reward determined by the reward function  $R(s, a)$ . The discount factor  $\gamma \in [0, 1]$  measures the importance of future rewards. The goal of the agent is to find an optimal policy  $\pi_\phi(a|s)$ , which is able to select the best action  $a$  in each state  $s$  to maximize the expected return  $J(\phi)$ :

$$J(\phi) = E_{\tau \sim \pi_\phi} [R(\tau)] \quad (5)$$

where  $\tau = (s_0, a_0, s_1, \dots, a_{T-1}, s_T)$  denotes a  $T$ -step trajectory. Through continuous interactions with the environment, the agent can gradually refine its strategy for determining the axial control points of the free-form pipe.

## 4. Methodology

### 4.1. Environment modeling

The layout space in an aeroengine is defined by the casing and nacelle surfaces, both of which can be considered as revolution surfaces generated by rotating their respective generatrices,  $\rho = f_c(z)$  and  $\rho = f_n(z)$  around the  $z$ -axis. As illustrated in Fig. 2, the layout space can be expressed as:

$$\begin{cases} f_c(z) \leq \rho < f_n(z) \\ 0 \leq \theta < 2\pi \\ z_{\min} \leq z < z_{\max} \end{cases} \quad (6)$$

where  $z$ ,  $\rho$ , and  $\theta$  represent the axes of the cylindrical coordinate system, while  $z_{\max}$  and  $z_{\min}$  denote the upper and lower bounds of the layout space on the  $z$ -axis, respectively.

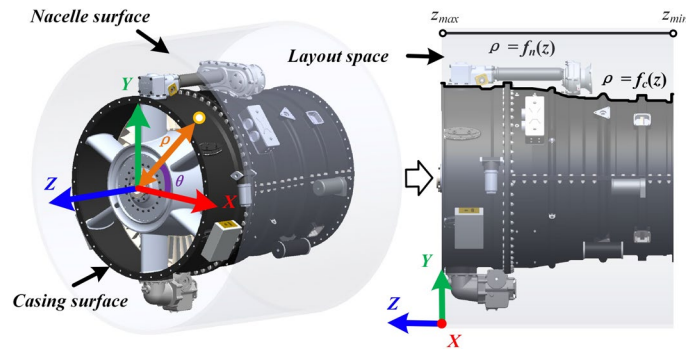


**Fig. 2.** Space of pipe routing in aeroengine.

Within the layout space, various obstacles, such as electrical equipment, fuel tanks, and maintenance areas, restrict the permissible paths for pipes. These obstacles often have irregular shapes, posing challenges for collision detection. Existing research commonly employs bounding boxes to approximate obstacles with simplified geometries. In this study, we adopt an octree-based modeling approach to balance geometric accuracy and computational efficiency [23]. As illustrated in Fig. 4, obstacles in CAD software are typically represented as solid models. By sampling these solid models, point cloud data can be generated, which can then be converted into a voxel-based representation using the octree method. The steps of the octree-based modeling method in the cylindrical

coordinate system  $(z, \rho, \theta)$  are detailed in Fig. 4. First, the upper and lower bounds of obstacle point clouds in the cylindrical coordinate system are utilized to define the initial modeling space, which acts as the root node of the octree. The initial space is then subdivided into  $2^3$  equal subspaces, referred to as the leaf nodes of the octree. Each subspace is classified as an obstacle subspace, marked by black, if it contains at least one point; otherwise, it is designated as free space and left blank. Free subspaces remain unchanged, while each obstacle subspace is treated as a new root node and recursively subdivided until the maximum division depth is reached. The maximum division depth is a parameter to balance modeling accuracy and computational efficiency. While a larger division depth enhances the precision of obstacle representation, it also increases the computational cost.

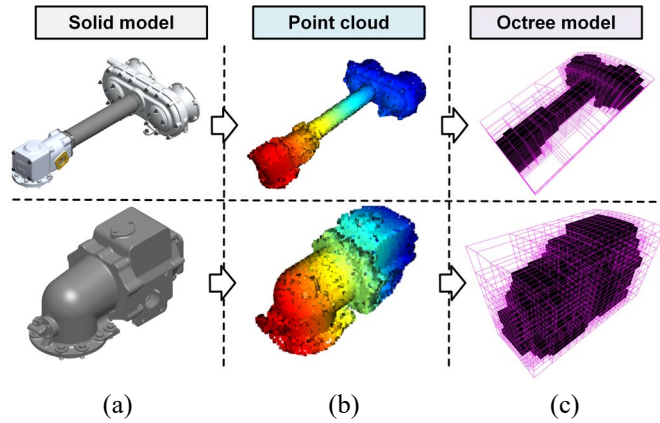


**Fig. 3.** Representation of obstacles through octree-based modeling approach. (a) Solid model; (b) Point cloud; (c) Octree model.

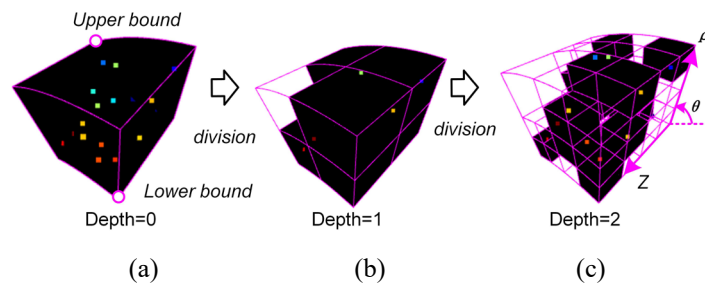


**Fig. 4.** Steps for octree-based modeling in cylindrical coordinate system. (a) Depth=0; (b) Depth=1; (b) Depth=2.

#### 4.2. Unified rule modeling framework

Pipe routing is governed by numerous layout rules, which can be broadly categorized into layout objectives and layout tendencies, as illustrated in Fig. 5. Layout objectives define clear, quantifiable metrics that reflect the optimization goals of the pipe routing, such as minimizing pipe length, weight, number of bends, and manufacturing costs. Conversely, layout tendencies describe spatial positioning preferences between the pipes and external components. These tendencies can be further divided into deterministic and fuzzy rules based on their level of clarity. Deterministic rules provide explicit, quantifiable constraints, such as maintaining a minimum gap between pipes and obstacles. In contrast, fuzzy rules are more elastic or ambiguous and difficult to be quantified. For example, a fuzzy rule might specify that pipes should be routed as close as possible to the casing surface or nearby accessories. These rules represent only a fraction of the complexities involved in practical aeroengine pipe routing. Real-world scenarios may involve dozens or even hundreds of rules, with additional customization requirements introducing unique constraints for different engine designs. Consequently, the development of a unified framework for rule modeling becomes essential.

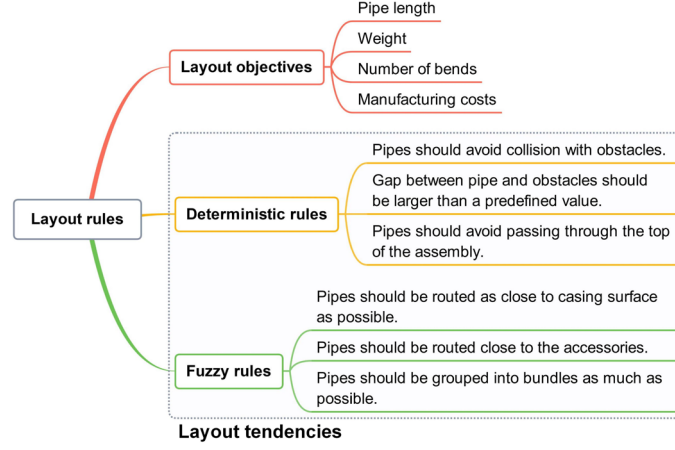


**Fig. 5.** Layout rules of pipe routing in aeroengine.

Inspired by the artificial potential field method [45], potential energy is utilized to represent layout tendencies in a unified framework. The objects external to the pipe in the layout preference rules, such as obstacles, casing surfaces, or previously laid pipes, are collectively referred to as external components (ECs). For an EC where proximity to the pipe is undesirable, a repulsive potential field is generated, mathematically expressed as:

$$U_r(P_{a,i}) = k_r, \quad P_{a,i} \in Z_r \quad (7)$$

where  $P_{a,i}$  denotes the  $i$ -th point on the pipe axis, and  $k_r$  represents the repulsive gain factor, a negative value that defines the maximum strength of the repulsive potential field, while  $Z_r$  specifies its influence zone. The repulsive field penalizes the pipe with negative potential energy when it enters an impermissible region. Conversely, for an EC that encourages proximity to the pipe, an attractive potential field is generated around it, mathematically defined as:

$$U_a(P_{a,i}) = k_a \times \frac{d_{\max} - d(P_{a,i}, EC)}{d_{\max} - d_{\min}}, \quad P_{a,i} \in Z_a \quad (8)$$

where  $k_a$  is the attractive gain factor, a positive value that defines the maximum strength of the attractive potential field.  $Z_a$  specifies the influence zone of this field, with  $d_{\min}$  and  $d_{\max}$  representing the closest and farthest distances between  $Z_a$  and EC, respectively. The function  $d(P_{a,i}, EC)$  denotes the distance between  $P_{a,i}$  and EC. Eq. (8) illustrates that the potential energy decreases gradually from  $k_a$  to 0 as a point within  $Z_a$  moves from the nearest to the farthest position relative to EC. Since an EC may produce both attractive and repulsive fields in different regions, the potential energy field for the  $j$ -th EC can be represented in a unified form as:

$$U_j(P_{a,i}) = \begin{cases} U_{a,j}(P_{a,i}), & P_{a,i} \in Z_{a,j} \\ U_{r,j}(P_{a,i}), & P_{a,i} \in Z_{r,j} \\ 0, & P_{a,i} \notin Z_{a,j} \cup Z_{r,j} \end{cases} \quad (9)$$

Each EC generates a potential field,  $U_j$ , based on the specified layout rules. The total potential energy at the point  $P_{a,i}$  is calculated as the superposition of the potential fields generated by all ECs, expressed as:

$$U(P_{a,i}) = \sum_{j=1}^m U_j(P_{a,i}) \quad (10)$$

where  $m$  represents the total number of ECs.

#### 4.3. Potential energy table

The computation of  $d(P_{a,i}, EC)$  is particularly time-intensive, especially when EC is an obstacle. Leveraging the octree-based modeling approach, this process is simplified to calculate the shortest distance between  $P_{a,i}$  and individual obstacle subspaces, represented as simple sectors. Nevertheless, pipe routing still involves frequent evaluations of  $d(P_i, EC)$ , significantly reducing the efficiency of layout optimization. To address this, the computation of  $d(P_{a,i}, EC)$  is performed prior to the optimization process. Specifically, the layout space is discretized into uniform fan-shaped grid cells of size  $s$ , as illustrated in Fig. 6. Each grid cell is

represented by its center coordinates, and the potential values for all grid cells are calculated and stored in a three-dimensional potential energy table,  $P_e$ , for future reference. Fig. 6 (c) provides a visualization of the potential energy distribution as point clouds. Because of the uniform grid division, the position index of  $P_{e,i}$  in the potential table can be easily determined using the following equation:

$$\begin{cases} i_z = \lfloor (z_i - z_{min}) / s \rfloor \\ i_\rho = \lfloor (\rho_i - \rho_{min}) / s \rfloor \\ i_\theta = \lfloor \theta_i \times \rho_{min} / s \rfloor \end{cases} \quad (11)$$

where  $\lfloor \cdot \rfloor$  denotes rounding down;  $i_z$ ,  $i_\rho$ , and  $i_\theta$  denote the potential energy indexes along the  $z$ -axis,  $\rho$ -axis, and  $\theta$ -axis, respectively;  $z_{min}$  and  $\rho_{min}$  represent the lower bounds of the layout space along the  $z$ -axis and the  $\rho$ -axis. The potential energy of point  $P_{e,i}$  can be efficiently queried through these indexes, expressed as  $P_{e,i} = P_e(i_z, i_\rho, i_\theta)$ , which eliminates the time-consuming step of calculating the potential energy, thus significantly enhancing the optimization efficiency.

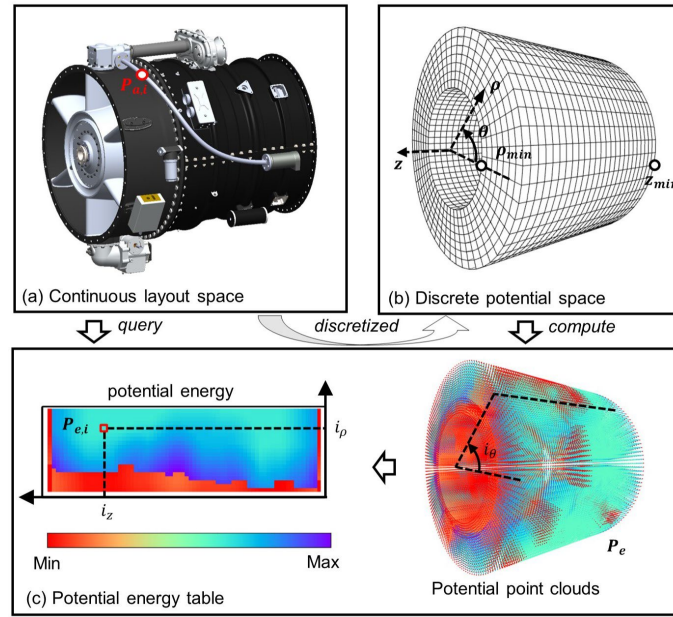


**Fig. 6.** Construction and querying of potential energy table. (a) Continuous layout space; (b) Discrete potential space; (c) Potential energy table.

#### 4.4. Self-learning pipe routing with NURBS curve

The PPO algorithm is utilized as the core method to optimize the policy  $\pi_\phi(a|s)$  of pipe routing. It is also combined with a fine-tuning approach to adapt to dynamic layout environments, as illustrated in Fig. 7. PPO is an on-policy, actor-critic algorithm that effectively balances training stability and computational efficiency. In PPO, the actor represents the learned policy that selects actions, while the critic evaluates the policy by estimating the state-value function  $V(s)$ . The algorithm optimizes a clipped surrogate objective, which constrains policy updates to ensure stable training. The loss function of the actor-network is defined as follows:

$$L_{\text{actor}}(\phi) = \mathbb{E}_i \left[ \min \left( r_i(\phi) \hat{A}_i, \text{clip}(r_i(\phi), 1 - \varepsilon, 1 + \varepsilon) \hat{A}_i \right) \right] \quad (12)$$

where  $r_i(\phi) = \frac{\pi_\phi(a_i|s_i)}{\pi_{\phi_{old}}(a_i|s_i)}$  is the probability ratio, with  $\phi_{old}$  being the policy parameters prior to the update.  $\varepsilon$  is a hyperparameter that controls the magnitude of policy updates. The advantage estimate  $\hat{A}_i$  is computed using generalized advantage estimation (GAE) and is expressed as:

$$\hat{A}_i = \delta_i + (\gamma\lambda)\delta_{i+1} + \dots + (\gamma\lambda)^{n-i+1} \delta_{n-1} \quad (13)$$

where  $\lambda$  is a hyperparameter that balances the trade-off between bias and variance, and  $\delta_i = r_i + \gamma V(s_{i+1}) - V(s_i)$  represents the

temporal difference error. The critic loss evaluates the accuracy of the value function in approximating the true state value. A commonly used metric is the mean squared error between the predicted value  $V_w(s_i)$  and the target value  $V_{target}(s_i)$ , formulated as:

$$L_{critic}(\omega) = \mathbb{E}_t \left[ (V_\omega(s_i) - V_{target}(s_i))^2 \right] \quad (14)$$

with  $w$  being the parameters of the critic network.

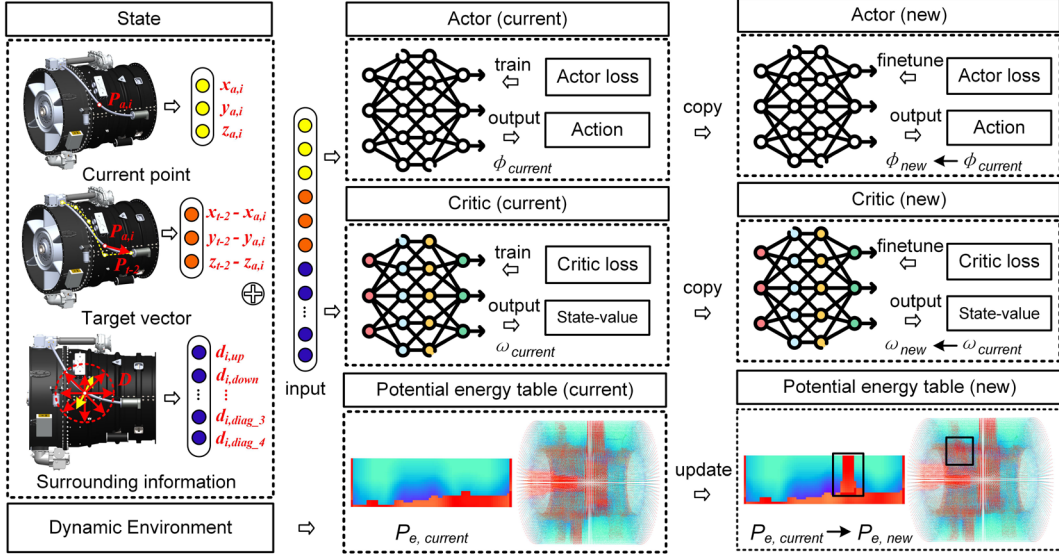


Fig. 7. Framework of self-learning pipe routing.

The configuration of the state space, action space, and reward function is crucial for the convergence speed and training performance of PPO. As illustrated in Fig. 7, the state space of the agent consists of three main parts, represented as:

$$S_i = [P_{a,i}, P_t - P_{a,i}, D_i] \quad (15)$$

where  $P_{a,i} = (x_{a,i}, y_{a,i}, z_{a,i})$  denotes the current position of the agent, initialized as  $P_s$  at the  $i = 0$ .  $P_t - P_{a,i}$  represents the layout task information.  $D = [d_{i,up}, d_{i,down}, \dots, d_{diag_3}, d_{diag_4}]$  captures the surrounding information of the agent, comprising the distances to the impassable region along the upward, downward, forward, backward, left, right, and four diagonal directions in space. The three components are concatenated and utilized as input to the PPO model.

During the PPO search process, cubic NURBS curves are employed to generate pipe paths. As a minimum of four control points is required for the generation of cubic NURBS curves,  $P_0$  and  $P_1$  are derived by extending the pipe diameter and twice the pipe diameter along the normal direction of the  $P_s$  port, respectively. Similarly,  $P_{t-1}$  and  $P_{t-2}$  are determined by extending  $P_t$  in the same manner, as illustrated in Fig. 8. This setting ensures that the pipe path is tangent to the start and target ports. The  $P_s$ ,  $P_0$ , and  $P_1$  are considered as the initial control points with default weights of 1, while subsequent control points are sequentially obtained by defining the action space of the agent as follows:

$$A_i = [\Delta x_{i+1}, \Delta y_{i+1}, \Delta z_{i+1}, w_{i+1}] \quad (16)$$

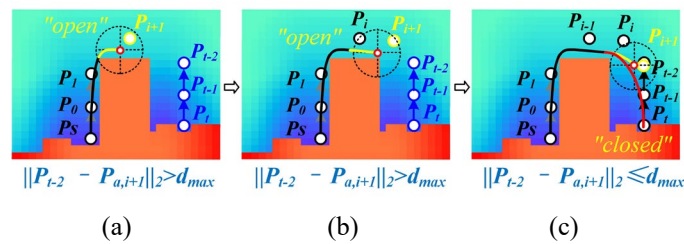


Fig. 8. Pipe routing using cubic NURBS curve. (a) Initial layout; (b) Intermediate process; (c) Termination when finding the target.

Once the action  $A_i$  is determined, the next control point  $P_{i+1}$  is calculated as  $P_{i+1} = P_i + (\Delta x_{i+1}, \Delta y_{i+1}, \Delta z_{i+1})$ , with the weight of  $P_{i+1}$  set to  $w_{i+1}$ . The new control point  $P_{i+1}$  is then appended to the list of control points  $P$ . By manipulating the knot vectors of

NURBS, a new segment of an open curve, which is not tangent to the line  $P_t P_{i+1}$ , is generated at the end of the last curve. The distance between the  $P_{a,i}$  and  $P_{t-2}$  is evaluated, and if it is larger than a predefined threshold,  $d_{max}$ , the search process continues. Otherwise, the target point is deemed reached, and  $P_{t-2}$ ,  $P_{t-1}$  and  $P_t$  are appended to  $P$  with weights of 1 to form a closed curve tangent to the line  $P_{t-1} P_t$ , thus seamlessly connecting  $P_s$  and  $P_t$ .

Whenever a new control point is identified, the corresponding curve segment is evaluated using the reward function. To prevent abnormal behaviors such as greed, timidity, and recklessness arising from reward sparsity, five distinct reward functions are designed. The first reward function,  $R_1$ , encourages the pipe path to approach the target point and is expressed as:

$$R_1 = \|P_{t-2} - P_{a,i}\|_2 - \|P_{t-2} - P_{a,i+1}\|_2 \quad (17)$$

$R_1$  rewards the agent when it moves closer to the target point compared to its previous position; otherwise, it imposes a penalty. Another reward function,  $R_2$ , incorporates the pipe length as a critical pipe layout objective and is expressed as:

$$R_2 = -l_{i+1} \quad (18)$$

where  $l_{i+1}$  denotes the length of the new curve segment. To ensure the pipe adheres to layout rules, the potential energy of the curve is also evaluated. Specifically, sampling at equal intervals  $\Delta l$  along the curve segments, the potential energy  $P_{e,j}$  is calculated at each sampling point. Based on this, two additional rewards,  $R_3$  and  $R_4$ , are defined as follows:

$$R_3 = \text{sum}(P_{e,j} | P_{e,j} < 0) \quad (19)$$

$$R_4 = \begin{cases} \text{mean}(P_{e,j} | P_{e,j} \geq 0) - \max(P_e), & P_{e,j} \notin \emptyset \\ 0, & \text{otherwise} \end{cases} \quad (20)$$

Here,  $R_3$  penalizes sampling points that enter impassable regions ( $P_{e,j} < 0$ ). In contrast,  $R_4$  defines the reward for points with  $P_{e,j} \geq 0$  by averaging their potential energies and subtracting  $\max(P_e)$ . The mean and maximum operations in  $R_4$  ensure its value remains negative, thereby discouraging greedy agent behavior. Finally, when the distance between the  $P_{a,i}$  and  $P_{t-2}$  is less than  $d_{max}$ , the target point is considered reached, and the agent receives the reward  $R_5$ , defined as:

$$R_5 = \begin{cases} 0, & \|P_{t-2} - P_{a,i+1}\|_2 > d_{max} \\ 1, & \|P_{t-2} - P_{a,i+1}\|_2 \leq d_{max} \end{cases} \quad (21)$$

In summary, the total reward function  $R$  is defined as a weighted sum of all sub-reward functions:

$$R = \mu_1 R_1 + \mu_2 R_2 + \mu_3 R_3 + \mu_4 R_4 + \mu_5 R_5 \quad (22)$$

where  $\mu_1, \mu_2, \mu_3, \mu_4$ , and  $\mu_5$  are the weights assigned to each sub-reward function.

In the pipe routing process, frequent modifications to engine design often necessitate re-routing the planned pipe, significantly increasing design man-hours. This study combines the fine-tuning method with PPO, as illustrated in Fig. 7. When the environment changes, the potential energy table is updated, and the parameters of the trained actor and critic model,  $\phi_{current}$  and  $\omega_{current}$ , are transferred to the new layout models. These parameters preserve the agent's previous search knowledge, enabling it to quickly adapt to the new layout environment through fine-tuning.

## 5. Experiments and results comparison

### 5.1. Experimental setup

To evaluate the performance of the proposed self-learning pipe routing (SLPR) framework, an aeroengine model was constructed using the computer-aided design software SolidWorks. The layout space was defined based on the designed casing generatrix  $f_c(z)$  and nacelle generatrix  $f_n(z)$ , which represent the upper and lower bounds of the layout space, respectively.  $f_c(z)$  is a polynomial function with a minimum value of 418.75, while  $f_n(z)$  is a constant set to 800. A total of 11 obstacles were designed in the aeroengine model, and their point clouds were exported to construct the potential energy table  $P_e$ . The cell size  $s$  of  $P_e$  was set to the pipe

diameter, the repulsive gain factor  $k_r$  to  $-1$ , and the attractive gain factor  $k_a$  to  $0.2$ .

The pipe routing experiments were then conducted in a Python-based simulation environment. The SLPR networks were implemented in PyTorch and trained on a cloud platform equipped with a 32 vCPU AMD EPYC 9654 96-Core Processor. The main hyperparameter settings of SLPR are summarized in Table 1. Three comparative experiments were conducted across different scenarios, including a comparison with constant-curvature pipe routing; a layout performance comparison with other algorithms, and a layout performance test in a dynamic environment. The simulation results are analyzed in detail below.

**Table 1**

Summary of model hyperparameter configurations in SLPR.

Parameter	Settings
Total training episodes	5000
Maximum steps per episode	20
Hidden layers of each MLPs	2
Neurons of each hidden layers	256
Discount factor $\gamma$	0.9
GAE factor $\lambda$	0.98
Clip ratio $\epsilon$	0.2
Weights $[\mu_1, \mu_2, \mu_3, \mu_4, \mu_5]$	$[0.01, 0.002, 0.05, 1, 10]$
Optimizer type	Adam
Learning rate of actor	$1 \times 10^{-4}$
Learning rate of critic	$5 \times 10^{-4}$
Judgment threshold $d_{max}$	100 mm
Sampling interval $\Delta l$	5 mm

## 5.2. Comparison of pipe types

Currently, aeroengine pipe routing primarily relies on constant-curvature pipes, which often lead to redundant segments, increased pipe length, and greater space occupation. This study proposes the use of free-form pipes based on NURBS curves, offering a more effective solution for the annular layout space of aeroengines. To evaluate the advantages of free-form pipes, comparative tests were conducted with constant-curvature pipes. Specifically, three constant-curvature pipe routing schemes were generated using the SolidWorks layout plug-in, with the pipe diameter set to 27 mm. Subsequently, the SLPR framework developed in this study was applied to derive free-form pipe routing schemes based on NURBS curves for identical pipe configurations.

The comparison of layout lengths between free-form pipes and constant-curvature pipes is presented in Table 2. The results reveal that free-form pipes exhibit significantly shorter layout lengths compared to constant-curvature pipes across all three configurations. Visualization of the layout schemes for these two pipe types is provided in Fig. 9. Free-form pipes demonstrate distinct advantages in aeroengine pipe routing within the specialized annular space, particularly in scenarios involving long-distance placement and obstacle avoidance. These advantages include reduced pipe length and complexity. For constant-curvature pipes, the flexibility is limited by the number of bends. While increasing the number of bends enhances flexibility, it also significantly complicates the manufacturing process. In contrast, the cubic NURBS curves employed in this study offer smooth routing solutions for free-form pipes, ensuring  $C^2$  continuity and facilitating the pipe-forming process.

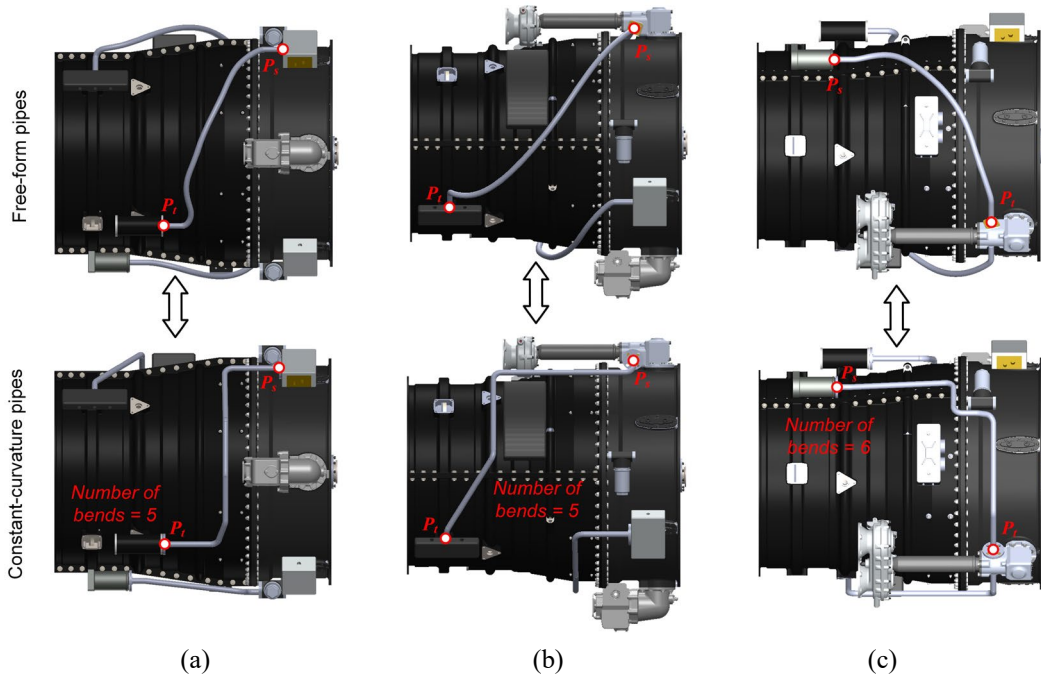


**Fig. 9.** Visualization of the layout schemes for different pipe types. (a) Pipe-1; (2) Pipe-2; (3) Pipe-3.

**Table 2**

Comparison of layout lengths for different pipe types.

Methods	Pipe-1 length (mm)	Pipe-2 length (mm)	Pipe-3 length (mm)
Constant-curvature pipe	1404.66	1812.20	1267.43
Free-form pipe (SLPR)	1174.02	1460.82	1148.50

### 5.3. Comparison of layout performance

In this subsection, three representative methods were selected to evaluate the performance of the proposed SLPR through comparative experiments in a static design environment. These methods include SAC, B-spline RRT\* (BSRRT\*), and quantum particle swarm optimization (QPSO), corresponding to RL algorithms, sampling-based search algorithms, and heuristic optimization algorithms, respectively. The details of each method are described below.

#### (1) SAC

The SAC is an off-policy actor-critic RL method designed for solving complex control tasks in continuous action spaces [38]. It combines value-based and policy-based techniques and employs the maximum entropy framework to maximize both the expected reward and policy entropy. The entropy regularization coefficient is initially set to 0.12 and is automatically adjusted during training to balance exploration and exploitation. Other parameter settings for SAC are consistent with those outlined in Section 5.1.

#### (2) BSRRT\*

The RRT\* algorithm is an optimized extension of the RRT algorithm. It searches for a path by extending an exploration tree from the root node to the target and enhances path quality through rewiring and reselecting the optimal parent node. The BSRRT\* algorithm, a recently proposed variant of RRT\*, is specifically designed for path planning based on piecewise quadratic B-spline [25], making it a suitable benchmark for comparison with the proposed SLPR. BSRRT\* also integrates an expanded candidate strategy and a goal-biased strategy to accelerate convergence. In this experiment, the cubic B-spline curves were used instead to accommodate the 3D layout environment, while other parameters remain consistent with those described in the original paper.

#### (3) QPSO

PSO is a widely used population-based intelligent optimization algorithm inspired by the collective behavior of organisms in nature. QPSO introduces the quantum mechanics theory into the PSO algorithm, reducing the number of tunable parameters while enhancing the optimization performance [46]. Within QPSO, particles are represented as a collection of coordinates and weights for all control points, with the number of control points fixed at 10. The optimal solution is found through cooperation and interaction among particles. The swarm size is set to 30, and the number of iterations is set to 1000, ensuring a balance between efficiency and

performance.

To enable a comprehensive performance comparison, ten distinct pipe routing tasks were designed within the aeroengine model, each with a pipe diameter of 19 mm. These tasks cover scenarios such as short-distance unobstructed layouts, long-distance layouts, and obstacle avoidance in narrow spaces. The evaluation metrics included pipe length, average potential energy of sampling points, number of rule-violating sampling points, number of successful tasks, number of control points, and computational time. These metrics assess the performance in terms of pipe length reduction, adherence to layout rules, path complexity, and computational efficiency. To ensure fairness, all methods were executed within the same computational environment.

The pipe routing results for SLPR are given in Fig. 10. As shown in the figure, for short-distance unobstructed layout tasks, including pipes 2 and 4, SLPR generates short and straight paths to minimize pipe length. For long-distance layout tasks, such as pipes 1 and 3, SLPR provides smooth, curved paths that conform to the annular surface of the aeroengine. In scenarios requiring obstacle avoidance, such as pipes 5, 6, and 7, SLPR successfully routes pipes around obstacles while avoiding passage over the top of obstacles, which adheres to the layout rules and demonstrates the effectiveness of the potential energy table in standardizing the pipe routing. Finally, for layout tasks in narrow spaces requiring obstacle avoidance, including pipes 8, 9, and 10, SLPR still provides feasible, collision-free paths, showcasing its robust search capabilities.

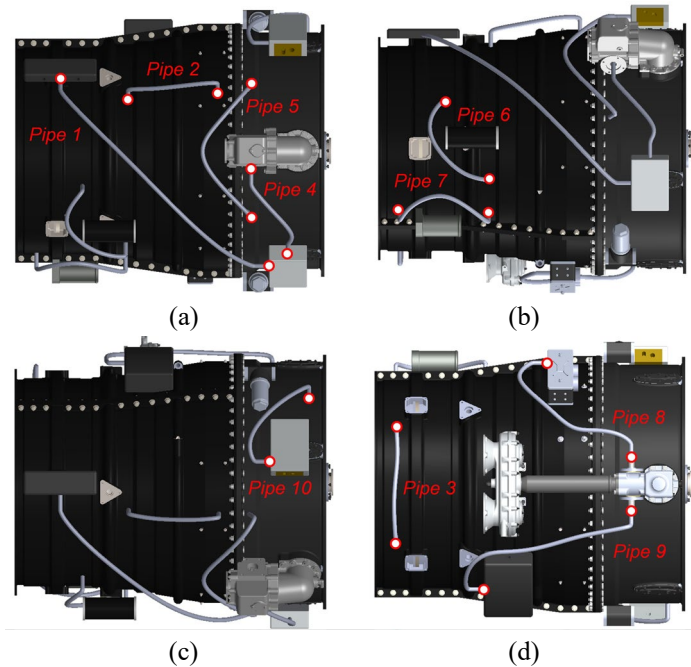


**Fig. 10.** Results of the free pipe routing for SLPR. (a) View 1; (b) View 2; (3) View 3; (4) View 4.

The comparison of average performance metrics for SLPR and other algorithms across the ten layout tasks is presented in Table 3, with the best results highlighted in bold. The results clearly demonstrate that SLPR outperforms all other methods in nearly every metric, except for a slight disadvantage in average potential energy (-0.16) compared to QPSO. SLPR successfully finds the shortest collision-free pipe paths that adhere to the layout rules across all the tasks, with a pipe length of 670.48 mm, zero violation points, and ten successful tasks. Meanwhile, SLPR demonstrates optimal computational efficiency, with an average routing time of 6.88 minutes, and exhibits the lowest path complexity, with an average of five control points, which is favorable for the manufacturing of free-form pipes.

**Table 3**

Performance of SLPR and several comparative methods on free pipe routing.

Metrics	SLPR	SAC	BSRRT*	QPSO
Length (mm)	<b>670.48</b>	733.73	980.15	1495.07
Average potential energy	-0.16	-0.40	-0.21	<b>-0.15</b>
Num of violation points	<b>0</b>	25.80	1.5	<b>0</b>
Successful times	<b>10</b>	9	<b>10</b>	<b>10</b>
Num of control points	<b>5</b>	7	9	10
Computation time (min)	<b>6.88</b>	11.20	11.68	11.82

A detailed comparison of the results for each tube, including pipe length, number of violation points, average potential energy, and number of control points, is presented in the line chart in Fig. 11. The RL algorithms, SLPR and SAC, outperform BSRRT\* and QPSO in optimizing pipe length. Nevertheless, it is noted that the obstacle-avoidance performance of the SAC algorithm is unstable, with violation points occurring in half of the layout tasks, leading to the worst performance in terms of average potential energy. The BSRRT\* algorithm performed well on tasks where the start and end points were close, such as pipes 2, 4, 7, and 10, but resulted in a violation on task 6. For pipes 2 and 10, BSRRT\* identified the simplest pipe paths that met the requirements with a small number of control points. However, for longer layout tasks, the generated paths contained too many control points, resulting in overly complex pipe paths with redundant segments. This is because the RRT\* algorithm generates the tree by randomly sampling points, which can lead to locally congested paths or unnecessary detours during tree expansion. The QPSO algorithm yields the best results in terms of average potential energy and successfully finds collision-free pipe paths across all tasks, excelling in adherence to layout rules. However, while QPSO can find feasible paths, they are not always optimal, particularly for pipes 3, 7, 8, and 9, where path redundancy is significant. This issue arises from the unique coding pattern of the heuristic algorithm, in which particles are represented by concatenating the coordinates and weights of all control points. Since the dimensions of the particles are fixed, the number of control points must be determined in advance. Fewer control points may result in paths that fail to bypass obstacles, while too many control points increase the difficulty of particle search and impair the optimization performance of QPSO. Therefore, selecting an appropriate number of control points according to the layout task is essential for QPSO.

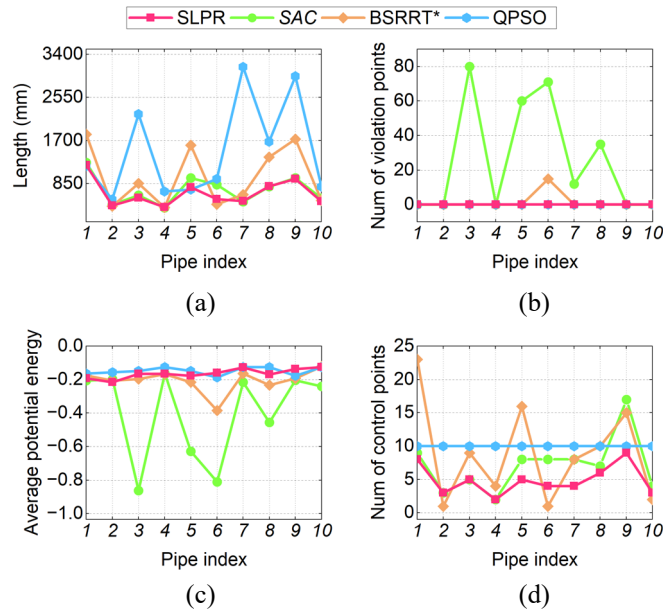


**Fig. 11.** Performance comparison for each pipe. (a) Length; (b) Num of violation points; (c) Average potential energy; (d) Num of control points.

In summary, the results clearly demonstrate that the proposed SLPR outperforms SAC, BSRRT\*, and QPSO in pipe routing capabilities. SLPR not only identifies the shortest collision-free pipe path that satisfies the layout rules with the fastest speed but also exhibits the lowest path complexity, facilitating easier pipe forming. These advantages make SLPR highly applicable to pipe routing and manufacturing in real-world scenarios.

#### 5.4. Comparison in dynamic environments

In real-world scenarios, aeroengines usually involve frequent design modifications, such as the addition, removal, or relocation of accessories. These modifications may result in collisions in the previously planned pipe layouts or degrade optimal solutions to suboptimal ones. In such cases, traditional search and heuristic algorithms must restart the pipe routing from scratch, significantly increasing design time and effort. In contrast, the self-learning-based SLPR retains the search knowledge from previous environments through the neural network parameters, allowing it to adapt to new layout environments with fine-tuning. This subsection

presents layout experiments in a dynamic design environment, using piping task 9 described in Section 5.3 as an example.

Two scenarios are specifically designed for evaluation. In the first scenario, a new obstacle is introduced to the originally planned pipe paths, causing collisions. In the second scenario, the obstacles are modified, requiring further refinement of the layout scheme, as shown in Fig. 12. To adapt to these changes, the potential energy table is first updated. The SLPR model, trained in the previous environment, is then directly applied for pipe routing in the new environment, as illustrated in the middle column of the figure. It can be seen that the previous agent is able to respond to the new environment. In the “New obstacle” scenario, the agent still provides a collision-free path, though it fails to reach the target point. In the “Modified Obstacle” scenario, the pipe path slightly adapts to the changed obstacle boundaries, resulting in a shorter pipe length. These results suggest that the agent can adapt to new environments based on prior knowledge, which can be further fine-tuned for improved performance.

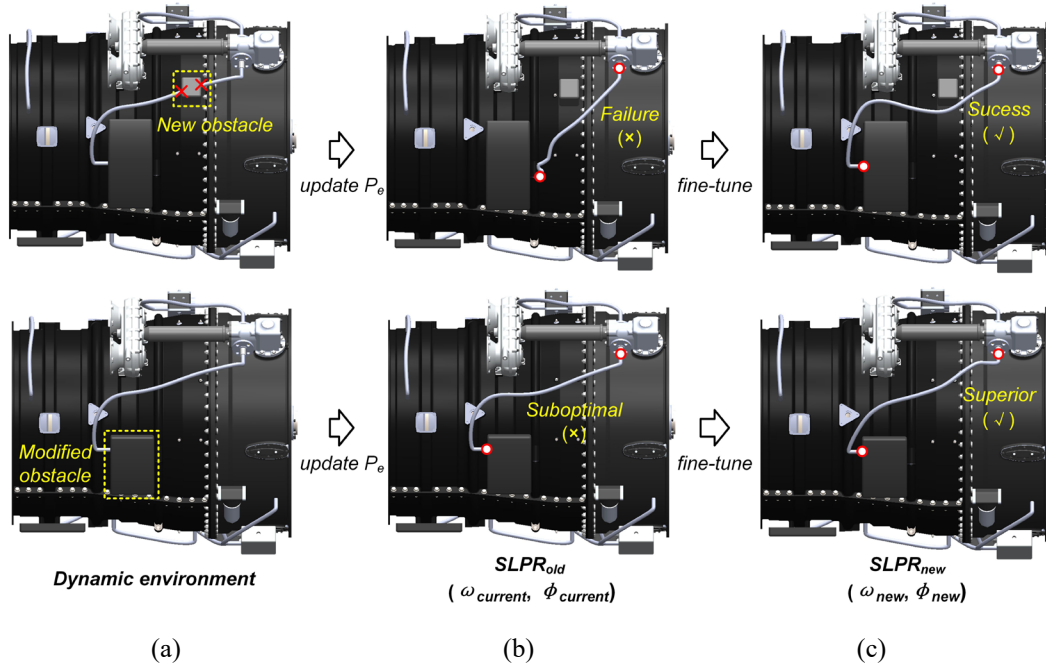


**Fig. 12.** Pipe routing in a dynamic environment. (a) “New obstacle” and “Modified Obstacle” scenarios; (b) Results of previously trained SLPR; (c) Results of fine-tuned SLPR.

The previously trained SLPR model was fine-tuned in the new environment using the updated potential energy table, while maintaining all parameters consistent with those described in Section 5.1, except for the total training episodes, which were set to 100. The visualization results of the fine-tuning are presented in the third column of Fig. 12. After fine-tuning, the pipe successfully bypasses the new obstacle and reaches the target point, while the pipe in the “Modified Obstacle” scenario achieves a shorter length. Furthermore, the iterative curves of the maximum return achieved by the agent during the training are presented in Fig. 13. The fine-tuned model is compared with a retrained model to demonstrate the role of prior knowledge in dynamic environment layouts. In the figure, the green and red curves represent the maximum return during fine-tuning and retraining, respectively. The results clearly indicate that the fine-tuned model maintains a high return from the beginning of training. As iterations progress, the fine-tuned model achieves maximum returns of 7.61 and 6.57 at the 32nd and 49th episodes, respectively. In contrast, the retrained model in the “Modified Obstacle” scenario achieves a return similar to that of the fine-tuned model only after 2,257 episodes. In the “New Obstacle” scenario, the retrained model achieves a maximum return of 6.03, which is lower than the performance of the fine-tuned model. These results suggest that leveraging prior knowledge not only accelerates adaptation to new environments but also enhances the quality of the final solution.

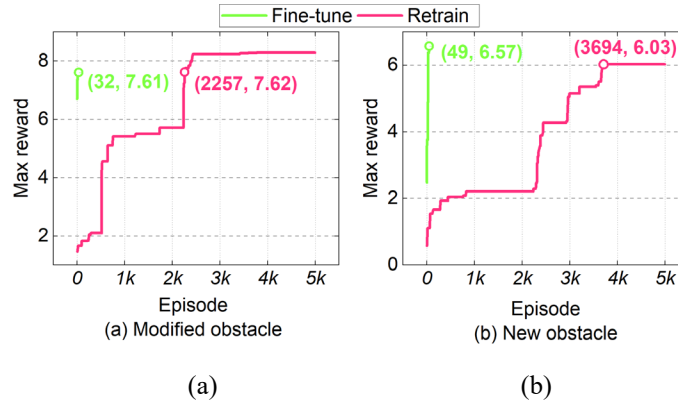


**Fig. 13.** Maximum return curves for fine-tuned and retrained models. (a) In “Modified obstacle” scenario; (b) In “New obstacle” scenario.

The performance comparison of SLPR, BSRRT\*, and QPSO in dynamic environments is presented in Table 4, in which BSRRT\* and QPSO were retrained to adapt to the new environment. The results indicate that SLPR only requires 24.18 seconds and 25.22 seconds to adapt to the new environment, respectively. This is significantly less than BSRRT\* and QPSO, which generally require over 700 seconds of computation time. In addition, the lengths of the pipe generated by SLPR are substantially shorter than those produced by BSRRT\* and QPSO, and no violation points are observed in the SLPR results.

To sum up, the SLPR proposed in this study demonstrates the capability to rapidly adapt to changes in aeroengine designs through fine-tuning, eliminating the need for a labor-intensive search from scratch and significantly reducing design man-hours. SLPR not only exhibits excellent performance in static design environments but also adapts quickly to dynamic environmental changes, offering an efficient and intelligent solution for pipe routing in aeroengines.

**Table 4**

Performance of SLPR and several comparative methods in a dynamic environment.

Scenarios	Metrics	SLPR (old)	SLPR (fine-tune)	BSRRT*	QPSO
New obstacle	Length (mm)	683.51	1003.47	2035.47	3069.76
	Num of violation points	0	0	0	0
	Computation time (s)	/	24.18	1030.39	2222.09
	Successful times	0	1	1	1
Modified obstacle	Length (mm)	957.32	877.71	868.10	2409.96
	Num of violation points	0	0	18	0
	Computation time (s)	/	25.22	706.69	1294.81
	Successful times	1	1	1	1

## 6. Conclusion

This study proposes a self-learning pipe routing (SLPR) framework, centered on the proximal policy optimization algorithm, for the layout planning of free-form pipes defined by NURBS curves in aeroengines. The SLPR integrates a unified rule modeling framework and a potential energy table, which address the challenges of obstacle detection and fuzzy rule modeling in continuous space, enabling efficient and precise querying of interference and pipe routing tendencies. Through interactions with the environment, the agent of SLPR continuously refines the layout scheme and accumulates layout knowledge. Based on this knowledge, the agent can quickly adapt to new design environments by updating the potential energy table and fine-tuning the parameters, thus avoiding the significant time and effort required for searching from scratch. Extensive experiments were conducted to evaluate the layout performance of SLPR. The main conclusions are as follows:

(1) Comparison with constant-curvature pipes reveals that free-form pipes offer distinct advantages in aeroengine pipe routing, particularly for tasks involving long-distance placement and obstacle avoidance. The utilization of cubic NURBS curves ensures smooth routing for free-form pipes, reducing both pipe length and complexity, thus facilitating the pipe-forming process.

(2) Experimental results in a static design environment demonstrate that the proposed SLPR outperforms SAC, BSRRT\*, and QPSO in pipe routing. Specifically, SLPR achieves a pipe length of 670.48 mm, zero violation points, ten successful tasks, and

optimal computational efficiency. SLPR not only adheres strictly to layout rules via the potential energy table but also exhibits the lowest path complexity, making it highly suitable for real-world pipe routing and manufacturing applications.

(3) Tests in a dynamic design environment show that SLPR can quickly adapt to changes in aeroengine designs in approximately 25 seconds through fine-tuning, eliminating the labor-intensive searches from scratch required by traditional search and heuristic methods. Furthermore, SLPR can even yield superior solutions than starting the search from scratch by leveraging prior knowledge.

These results demonstrate that SLPR is a highly applicable method for pipe routing and manufacturing in real-world scenarios. SLPR offers an efficient and intelligent solution for pipe routing, fulfilling the lightweight, precision, and sustainability requirements of modern aeroengine design. Future work will focus on integrating forming defect prediction models for free-form pipes and curvature constraints into the framework to smooth paths and enhance the manufacturability of the pipe.

### Acknowledgements

This paper is funded by the National Natural Science Foundation of China (52275274), the Joint Funds of the National Natural Science Foundation of China (U20A20287), the Pioneer and Leading Goose R&D Program of Zhejiang, China (2024C01197), the Public Welfare Technology Application Projects of Zhejiang Province, China (LGG22E050008), the State Key Laboratory of Intelligent Manufacturing Equipment and Technology Open Project, China (IMETKF2024007). Zhejiang Province leading innovative entrepreneurial team project (2022R01012).

### Competing Interests

Authors declare that they have no conflict of interest.

### Data and code availability

Data will be made available on request.

### References

- [1] Y.H. Yin, L.D. Xu, Z.M. Bi, H. Chen, C. Zhou, A Novel Human-Machine Collaborative Interface for Aero-Engine Pipe Routing, *IEEE Trans. Ind. Inform.* 9 (2013) 2187-2199. <https://doi.org/10.1109/tii.2013.2257805>.
- [2] Z.S. Chen, H. Guan, X.L. Yuan, T. Xie, P. Xu, Rule-based generation of HVAC duct routing, *Automation in Construction*. 139 (2022) 14. <https://10.1016/j.autcon.2022.104264>.
- [3] J.-H. Park, R.L. Storch, Pipe-routing algorithm development: case study of a ship engine room design, *Expert Systems with Applications*. 23 (2002) 299-309. [https://doi.org/10.1016/S0957-4174\(02\)00049-0](https://doi.org/10.1016/S0957-4174(02)00049-0).
- [4] C. Wang, Q. Liu, Projection and Geodesic-Based Pipe Routing Algorithm, *IEEE Transactions on Automation Science and Engineering*. 8 (2011) 641-645. <https://doi.org/10.1109/TASE.2010.2099219>.
- [5] C. Liu, L. Wu, G. Li, W. Xiao, L. Tan, D. Xu, J. Guo, AI-based 3D pipe automation layout with enhanced ant colony optimization algorithm, *Automation in Construction*. 167 (2024) 105689. <https://doi.org/10.1016/j.autcon.2024.105689>.
- [6] Z. Zhang, J. Wu, B. Liang, M. Wang, J. Yang, M. Muzamil, A new strategy for acquiring the forming parameters of a complex spatial tube product in free bending technology, *Journal of Materials Processing Technology*. 282 (2020) 116662. <https://doi.org/10.1016/j.jmatprotec.2020.116662>.
- [7] Z. Wang, Y. Lin, L. Qiu, S. Zhang, D. Fang, C. He, L. Wang, Spatial variable curvature metallic tube bending springback numerical approximation prediction and compensation method considering cross-section distortion defect, *The International Journal of Advanced Manufacturing Technology*. 118 (2022) 1811-1827. <https://doi.org/10.1007/s00170-021-08051-w>.
- [8] H. Mazaheri, S. Goli, A. Nourollah, A survey of 3D Space Path-Planning Methods and Algorithms, *ACM Comput. Surv.* 57 (2025) 32. <https://doi.org/10.1145/3673896>.
- [9] Y.F. Qu, D. Jiang, G.Y. Gao, Y.J. Huo, Pipe Routing Approach for Aircraft Engines Based on Ant Colony Optimization, *J. Aerosp. Eng.* 29 (2016) 10. [https://doi.org/10.1061/\(asce\)as.1943-5525.0000543](https://doi.org/10.1061/(asce)as.1943-5525.0000543).

- [10] L.X. Liu, X. Wang, X. Yang, H.J. Liu, J.P. Li, P.F. Wang, Path planning techniques for mobile robots: Review and prospect, *Expert Systems with Applications*. 227 (2023) 30. <https://doi.org/10.1016/j.eswa.2023.120254>.
- [11] Z. Zhang, Y. Zhang, R. Han, L. Zhang, J. Pan, A Generalized Continuous Collision Detection Framework of Polynomial Trajectory for Mobile Robots in Cluttered Environments, *IEEE Robotics and Automation Letters*. 7 (2022) 9810-9817. <https://doi.org/10.1109/LRA.2022.3191934>.
- [12] Z. Yao, W. Zhang, Y. Shi, M. Li, Z. Liang, Q. Huang, ReinforcedRimJump: Tangent-Based Shortest-Path Planning for Two-Dimensional Maps, *IEEE Trans. Ind. Inform.* 16 (2020) 949-958. <https://doi.org/10.1109/TII.2019.2918589>.
- [13] C. Liu, L. Wu, X. Huang, W. Xiao, Improved dynamic adaptive ant colony optimization algorithm to solve pipe routing design, *Knowledge-Based Systems*. 237 (2022) 107846. <https://doi.org/10.1016/j.knsys.2021.107846>.
- [14] L. Ren, X. Fan, J. Cui, Z. Shen, Y. Lv, G. Xiong, A Multi-Agent Reinforcement Learning Method With Route Recorders for Vehicle Routing in Supply Chain Management, *IEEE Transactions on Intelligent Transportation Systems*. 23 (2022) 16410-16420. <https://doi.org/10.1109/TITS.2022.3150151>.
- [15] K. Ma, S. Liao, Y. Niu, Connected vehicles' dynamic route planning based on reinforcement learning, *Future Generation Computer Systems*. 153 (2024) 375-390. <https://doi.org/10.1016/j.future.2023.11.037>.
- [16] Í. Elguea-Aguinaco, A. Serrano-Muñoz, D. Chrysostomou, I. Inziarte-Hidalgo, S. Bøgh, N. Arana-Arexolaleiba, A review on reinforcement learning for contact-rich robotic manipulation tasks, *Robotics and Computer-Integrated Manufacturing*. 81 (2023) 102517. <https://doi.org/10.1016/j.rcim.2022.102517>.
- [17] Z. He, L. Dong, C. Sun, J. Wang, Asynchronous Multithreading Reinforcement-Learning-Based Path Planning and Tracking for Unmanned Underwater Vehicle, *IEEE Transactions on Systems, Man, and Cybernetics: Systems*. 52 (2022) 2757-2769. <https://doi.org/10.1109/TSMC.2021.3050960>.
- [18] Z. Chu, Y. Wang, D. Zhu, Local 2-D Path Planning of Unmanned Underwater Vehicles in Continuous Action Space Based on the Twin-Delayed Deep Deterministic Policy Gradient, *IEEE Transactions on Systems, Man, and Cybernetics: Systems*. 54 (2024) 2775-2785. <https://doi.org/10.1109/TSMC.2023.3348827>.
- [19] J. Schulman, F. Wolski, P. Dhariwal, A. Radford, O. Klimov, Proximal policy optimization algorithms, in, 2017.
- [20] C. Liu, L. Wu, G.X. Li, H. Zhang, W.S. Xiao, D.P. Xu, J.J. Guo, W.T. Li, Improved multi-search strategy A\* algorithm to solve three-dimensional pipe routing design, *Expert Systems with Applications*. 240 (2024) 26. <https://doi.org/10.1016/j.eswa.2023.122313>.
- [21] Y. Lin, Q. Zhang, A multi-objective cooperative particle swarm optimization based on hybrid dimensions for ship pipe route design, *Ocean Engineering*. 280 (2023) 114772. <https://doi.org/10.1016/j.oceaneng.2023.114772>.
- [22] Q. Zhang, Y. Lin, Integrating multi-agent reinforcement learning and 3D A\* search for facility layout problem considering connector-assembly, *J. Intell. Manuf.* 35 (2024) 3393-3418. <https://doi.org/10.1007/s10845-023-02209-x>.
- [23] Y.F. Qu, D. Jiang, X.L. Zhang, A new pipe routing approach for aero-engines by octree modeling and modified max-min ant system optimization algorithm, *J. Mech.* 34 (2018) 11-19. <https://doi.org/10.1017/jmech.2016.86>.
- [24] M. Elbanhawi, M. Simic, R. Jazar, Randomized Bidirectional B-Spline Parameterization Motion Planning, *IEEE Transactions on Intelligent Transportation Systems*. 17 (2016) 406-419. <https://doi.org/10.1109/TITS.2015.2477355>.
- [25] H. Feng, Q. Hu, Z. Zhao, X. Feng, Smooth path planning under maximum curvature constraints for autonomous underwater vehicles based on rapidly-exploring random tree star with B-spline curves, *Engineering Applications of Artificial Intelligence*. 133 (2024) 108583. <https://doi.org/10.1016/j.engappai.2024.108583>.
- [26] Y. Liu, W. Zhao, R. Sun, X. Yue, Optimal path planning for automated dimensional inspection of free-form surfaces, *Journal of Manufacturing Systems*. 56 (2020) 84-92. <https://doi.org/10.1016/j.jmsy.2020.05.008>.
- [27] C. Yan, Y. Shi, Z. Li, S. Wen, Q. Wei, Chapter 2 - Software algorithm and route planning, in: C. Yan, Y. Shi, Z. Li, S. Wen, Q. Wei (Eds.) *Selective Laser Sintering Additive Manufacturing Technology*, Academic Press, 2021, pp. 123-249.
- [28] Y. Xu, X. Tong, U. Stilla, Voxel-based representation of 3D point clouds: Methods, applications, and its potential use in the construction industry, *Automation in Construction*. 126 (2021) 103675. <https://doi.org/10.1016/j.autcon.2021.103675>.

- [29] T. Ito, A genetic algorithm approach to piping route path planning, *J. Intell. Manuf.* 10 (1999) 103-114. <https://doi.org/10.1023/A:1008924832167>.
- [30] Z. Dong, X. Bian, Ship Pipe Route Design Using Improved A\* Algorithm and Genetic Algorithm, *IEEE Access.* 8 (2020) 153273-153296. <https://doi.org/10.1109/ACCESS.2020.3018145>.
- [31] B. Cetinsaya, D. Reiners, C. Cruz-Neira, From PID to swarms: A decade of advancements in drone control and path planning - A systematic review (2013–2023), *Swarm and Evolutionary Computation.* 89 (2024) 101626. <https://doi.org/10.1016/j.swevo.2024.101626>.
- [32] S. Liu, H. Jiang, S. Chen, J. Ye, R. He, Z. Sun, Integrating Dijkstra's algorithm into deep inverse reinforcement learning for food delivery route planning, *Transportation Research Part E: Logistics and Transportation Review.* 142 (2020) 102070. <https://doi.org/10.1016/j.tre.2020.102070>.
- [33] Z. Lin, K. Wu, R. Shen, X. Yu, S. Huang, An Efficient and Accurate A-Star Algorithm for Autonomous Vehicle Path Planning, *IEEE Transactions on Vehicular Technology.* 73 (2024) 9003-9008. <https://doi.org/10.1109/TVT.2023.3348140>.
- [34] J. Qi, H. Yang, H. Sun, MOD-RRT\*: A Sampling-Based Algorithm for Robot Path Planning in Dynamic Environment, *IEEE Transactions on Industrial Electronics.* 68 (2021) 7244-7251. <https://doi.org/10.1109/TIE.2020.2998740>.
- [35] S. Sandurkar, W. Chen, GAPRUS—genetic algorithms based pipe routing using tessellated objects, *Computers in Industry.* 38 (1999) 209-223. [https://doi.org/10.1016/S0166-3615\(98\)00130-4](https://doi.org/10.1016/S0166-3615(98)00130-4).
- [36] C. Wang, Z. Wang, S. Zhang, J. Tan, Adam-assisted quantum particle swarm optimization guided by length of potential well for numerical function optimization, *Swarm and Evolutionary Computation.* 79 (2023) 101309. <https://doi.org/10.1016/j.swevo.2023.101309>.
- [37] Y. Qu, D. Jiang, Q. Yang, Branch pipe routing based on 3D connection graph and concurrent ant colony optimization algorithm, *J. Intell. Manuf.* 29 (2018) 1647-1657. <https://doi.org/10.1007/s10845-016-1203-4>.
- [38] T. Haarnoja, A. Zhou, P. Abbeel, S. Levine, Soft Actor-Critic: Off-Policy Maximum Entropy Deep Reinforcement Learning with a Stochastic Actor, in: D. Jennifer, K. Andreas (Eds.) *Proceedings of the 35th International Conference on Machine Learning*, PMLR, *Proceedings of Machine Learning Research*, 2018, pp. 1861--1870.
- [39] A. Al-Hilo, M. Samir, C. Assi, S. Sharafeddine, D. Ebrahimi, UAV-Assisted Content Delivery in Intelligent Transportation Systems-Joint Trajectory Planning and Cache Management, *IEEE Transactions on Intelligent Transportation Systems.* 22 (2021) 5155-5167. <https://doi.org/10.1109/TITS.2020.3020220>.
- [40] M. Xi, J. Yang, J. Wen, Z. Li, W. Lu, X. Gao, An Information-Assisted Deep Reinforcement Learning Path Planning Scheme for Dynamic and Unknown Underwater Environment, *IEEE Transactions on Neural Networks and Learning Systems.* (2023) 1-12. <https://doi.org/10.1109/TNNLS.2023.3332172>.
- [41] J. Yang, J. Huo, M. Xi, J. He, Z. Li, H.H. Song, A Time-Saving Path Planning Scheme for Autonomous Underwater Vehicles With Complex Underwater Conditions, *IEEE Internet of Things Journal.* 10 (2023) 1001-1013. <https://doi.org/10.1109/JIOT.2022.3205685>.
- [42] Y. Kim, K. Lee, B. Nam, Y. Han, Application of reinforcement learning based on curriculum learning for the pipe auto-routing of ships, *Journal of Computational Design and Engineering.* 10 (2023) 318-328. <https://doi.org/10.1093/jcde/qwad001>.
- [43] X. Li, H. Zhao, X. He, H. Ding, A novel cartesian trajectory planning method by using triple NURBS curves for industrial robots, *Robotics and Computer-Integrated Manufacturing.* 83 (2023) 102576. <https://doi.org/10.1016/j.rcim.2023.102576>.
- [44] S.S. Richard, G.B. Andrew, The Reinforcement Learning Problem, in: *Reinforcement Learning: An Introduction*, MIT Press, 1998, pp. 51-85.
- [45] Y. Liu, C. Chen, Y. Wang, T. Zhang, Y. Gong, A fast formation obstacle avoidance algorithm for clustered UAVs based on artificial potential field, *Aerospace Science and Technology.* 147 (2024) 108974. <https://doi.org/10.1016/j.ast.2024.108974>.
- [46] J. Sun, B. Feng, W. Xu, Particle swarm optimization with particles having quantum behavior, in: *Proceedings of the 2004 Congress on Evolutionary Computation, CEC2004, 2004*, pp. 325-331.